CFD validation for flyash particle classification in hydrocyclones

K. Udaya Bhaskar [a,*], Y. Rama Murthy [a], N. Ramakrishnan [a],
J.K. Srivastava [b], Supriya Sarkar [c], Vimal Kumar [d]

[a] Regional Research Laboratory (CSIR), Bhopal, MP 462 026, India
[b] Chemical Engineering Department, Ujjain Engineering College, Ujjain 456 001, India
[c] Fluent India Pvt. Ltd., Pune 411 057, India
[d] Technology Information Forecasting Assessment Council, New Delhi 110 016, India

Abstract

The investigation pertains to establishing a simulation methodology for understanding the flyash classification characteristics of a 76 and 50 mm diameter hydrocyclone where the work was carried out using commercially available CFD software. Comparative results on the simulated and experimental water throughput, split values are presented. Results indicted that there is a good match in water split between the experimental and simulated values with error values below 10% at different hydrocyclone designs. Further a discussion is made on the flow features at comparable ratio of cyclone diameter to spigot opening in the 76 and 50 mm designs. The vertical core region around the cyclone axis having static pressure equal to or below the atmospheric pressure is examined to be increasing in diameter from bottom of the spigot opening till the interface where vortex finder joins the main cylindrical cyclone body and remains more or less similar at the vortex finder outlet. The diameter of this zone at the spigot outlet is 0.6 and 5.4 mm at 3.2 and 9.4 mm spigot openings in case of 50 mm diameter hydrocyclone. The diameter of the core at spigot outlet is found to be around 9.2 and 11 mm at 15 and 20 mm for spigot openings in case of 76 mm diameter hydrocyclone.

Classification of flyash particulates is simulated through discrete phase modeling using particles injection technique and the simulated results are further validated with suitably performed experiments. With 50 mm diameter hydrocyclone, reasonable predictions are observed at 9.4 mm spigot opening. Considerable deviation in particle distribution points with this hydrocyclone is observed at narrowest spigot diameter of 3.2 mm. The simulated values of d_{50} in case of 50 mm diameter hydrocyclone are 8 and 10 μm at 9.4 and 3.2 mm diameter spigot openings. Better predictions are obtained with 76 mm diameter hydrocyclone at both 10 and 15 mm diameter spigot openings. Similarly, the simulated d_{50} values are 14 and 20 μm at 15 and 10 mm diameter hydrocyclones. Possible reasons for deviations in the results relating the spigot opening, solids concentration at the underflow and in turn role of slurry viscosity on the air core diameter are proposed.

© 2006 Elsevier Ltd. All rights reserved.

Keywords: CFD simulation; Hydrocyclones; Flyash; Classification

1. Introduction

Hydrocyclone is a versatile unit operation for applications in liquid–liquid separation, liquid–solid separation, air–solid separation, and solid–solid separation. Due to several industrial advantages, like good separation efficiency, ease in operation, high throughput, less maintenance, less floor space requirement etc., the hydrocyclones are very popular in large number of industrial sectors like mineral processing, environmental, food processing, chemical engineering etc. The works related to understanding the principles began only in mid fifties (Kelsall, 1952) though the unit was originally invented in late 18th century. Kelsall's studies on the axial, radial and tangential

---

* Corresponding author. Tel.: +91 7552 471956; fax: +91 7552 488323.
E-mail address: kubhaskar2001@yahoo.com (K. Udaya Bhaskar).

velocity profiles formed the basis for subsequent research on hydrocyclones. Due to the complex phenomenon involved in analyzing flow behavior coupled with non-availability of high-speed computational systems most of the research works till the recent past were focused on the empirical modeling (Lynch and Rao, 1975; Plitt, 1976). These models are material specific and their applications are limited to the boundary conditions within which the model suitability is evaluated. However, the advent of high speed computational systems, in last couple of decades made researchers focus performance simulations using Computational Fluid Dynamics (CFD) techniques (Pericleous and Rhodes, 1986; Hsieh and Rajamani, 1988; Monredon et al., 1992; Rajamani and Milin, 1992; Dyakowski and Williams, 1993; Dyakowski et al., 1994, 1999; Malhotra et al., 1994; Hargreaves and Silvester, 1990; Devulapalli and Rajamani, 1996; Griffiths and Boysan, 1996; Slack and Wraith, 1997; Slack and Boysan, 1998; Stovin and Saul, 1998; Suasnabar and Fletcher, 1999; Slack et al., 2000, 2003; Ma et al., 2000; Nowakowski et al., 2000, 2004; Grady et al., 2002, 2003; Nowakowski and Dyakowski, 2003; Schuetz et al., 2004; Cullivan et al., 2003, 2004; Delgadillo and Rajamani, 2005; Narasimha et al., 2005, 2006; Udaya Bhaskar et al., in press). Gradual evolution has taken place from 2D axi-symmetric studies of hydroclones to 3D non-axisymmetric geometry simulation methodologies. Any numerical technique needs development of suitable methodology and extensive validation with the experimental data before its real applications in design and performance simulation. Among the reported studies, the validation was mostly carried out with water flow characteristics and only a few of them are related to solids separation behavior. The present study involves simulation of water flow behaviour at different design conditions of 50 and 76 mm diameter hydrocyclone and particle size distribution behaviour under both simulated and experimental conditions. Simulation was carried out using commercially available CFD software 'Fluent 6.1.22'. The simulation results on cyclone cut size d_{50} values at different spigot openings are validated with experimental data generated in the laboratory treating flyash at different concentration of solids in the feed slurry.

2. Model description

2.1. Geometry

Experimental and CFD simulation works are carried out on 76 and 50 mm diameter standard hydrocyclone geometries. The geometrical description is discussed separately as follows.

2.1.1. 76 mm hydrocyclone

The geometrical details of 76 mm hydrocyclone are presented in Table 1. The cylindrical body is 76 mm diameter and 85 mm in height with a closed end at the top surface

Table 1
Design details of 76 mm hydrocyclone

Dimensions (mm)	Cyclone 1	Cyclone 2	Cyclone 3	Cyclone 4
CD	76	76	76	76
CyL	85	85	85	85
VFD	25	25	25	25
VFL	90	90	90	90
FI (l × w)	20 × 10	20 × 10	20 × 10	20 × 10
CA*	10^0	10^0	10^0	10^0
SPD	10	15	20	25

CD, cyclone diameter; CyL, cylindrical length; VFD, vortex finder diameter; VFL, vortex finder length; FI, feed inlet dimensions (length × width); CA*, cone angle in degrees; SPD, spigot diameter.

and bottom face open. A frustum with a larger diameter of 76 mm and smaller diameter of 10 mm maintained at a cone angle of 10° is connected to the main cylindrical body with the 76 mm diameter face. A cylindrical vortex finder with an inner diameter of 25 mm and outer diameter of 40 mm protrudes into the main cylindrical body extending over a length of 60 mm inside and 30 mm above the top closed surface. A rectangular 20 × 10 mm tangential feed inlet opening is connected to the cylindrical surface at a height of 15 mm below the top surface. Studies were carried out on this geometry by changing the bottom diameter of the frustum at 10, 15, 20 and 25 mm at a constant cone angle of 10°.

2.1.2. 50 mm hydrocyclone

The geometrical details of 50 mm hydrocyclone used for simulation are also presented in Table 2. The cylindrical body is 50 mm diameter and 85 mm in height with a closed end at the top surface and bottom face open. A frustum with a larger diameter of 50 mm and smaller diameter of 3.2 mm maintained at a cone angle of 10° is connected to the main cylindrical body with the 50 mm diameter face. A cylindrical vortex finder with an inner diameter of 14.3 mm and outer diameter of 26 mm protrudes into the main cylindrical body extending over a length of 30 mm inside and 20 mm above the top closed surface. A square 7 × 7 mm tangential feed inlet opening is connected to the cylindrical surface at a height of 17 mm below the top surface. Studies were carried out on this geometry by changing

Table 2
Design details of 50 mm hydrocyclone

Dimensions (mm)	Cyclone 1	Cyclone 2	Cyclone 3	Cyclone 4
CD	50	50	50	50
CyL	85	85	85	85
VFD	14.3	14.3	14.3	14.3
VFL	50	50	50	50
FI (l × w)	7 × 7	7 × 7	7 × 7	7 × 7
CA*	10^0	10^0	10^0	10^0
SPD	3.2	4.5	6.4	9.4

CD, cyclone diameter; CyL, cylindrical portion length; VFD, vortex finder diameter; VFL, vortex finder length; FI, feed inlet dimensions (length × width); CA*, cone angle in degrees; SPD, spigot diameter.

the bottom diameter of the frustum at 3.2, 4.5, 6.4 and 9.4 mm at a constant cone angle of 10°.

2.2. Meshing scheme

Hydrocyclones truly cannot be modeled in a 2D plane due to non-axisymmetric nature at the feed inlet opening. Earlier reports also indicated that the results using a 3D model are better matching with the experimental data compared to the results with axisymmetric geometry [www.psl.bc.ca/downloads/presentations/cyclone/cyclone.html]. The present computational model is based on 3D geometry. Triangular mesh, which can fit into small acute angles in the geometry, is used to mesh the face that joins the inlet to the cylindrical cyclone body. This triangular mesh is then extruded in the vertical direction to give rise to wedge shaped control volumes in the tangential inlet region. The rest of the cyclone is meshed using unstructured hexahedral mesh, which is known to be less diffusive compared to other types of meshes like tetrahedra. A boundary layer mesh is generated adjacent to the outer wall of the cyclone. In order to capture the low-pressure central air-core, block-structured mesh is generated in that region. Additional care is taken to generate mesh near the spigot region where maximum aspect ratio is restricted to about 10. This is important to capture the back flow through spigot opening. Grid independence study was carried out with five different mesh densities with mesh sizes varying from 75,000 to 200,000. Water distribution studies have indicated that better predictions are obtained at higher mesh densities. A mesh density of 150,000 cells is optimized due to good predictions and reasonable computational time for simulations.

2.3. Boundary conditions

A velocity inlet condition is used to prescribe water-inflow through the rectangular cyclone feed inlet. The overflow and underflow outlets were designated as pressure outlets. The primary water phase (density = 998.2 kg/m^3 and viscosity = 1.003×10^{-6} kg/ms) enters the cyclone through the feed inlet. The outlet diameter at the underflow of 76 mm diameter hydrocyclone was varied at 10, 15, 20 and 25 mm. Similarly, the underflow outlet diameter was varied at 3.2, 4.5, 6.4, and 9.4 mm for the 50 mm hydrocyclone. For each of the above conditions, water flow behavior was simulated and further particle distribution characteristics were carried out using particle injection from the inlet surface. Inert solid spherical particles (density = 2300 kg/m^3) of different sizes varying from 1 to 100 μm were injected through the feed inlet. The flyash particles below 100 μm are completely spherical and hence no factors for shape correction are considered. The particles entering any of the pressure outlet zones were assigned to escape the vessel.

3. Numerical simulation

A segregated, steady state, 3D double precision implicit solver was used for simulating the flow and turbulence inside the hydrocyclone. The pressure interpolation scheme adopted was PRESTO (Pressure staggered option), which is useful for predicting highly swirling flow characteristics prevailing inside the cyclone body (Fluent Europe Ltd., 2002). In order to reduce the effects of numerical diffusion, higher order discretization schemes are recommended for simulating cyclones. Accordingly, a third order accurate QUICK scheme was used for spatial discretization. The SIMPLE algorithm was used for coupling the continuity and momentum equations. Turbulent flow inside a hydrocyclone is anisotropic in nature, hence choice of turbulence model is crucial. Within the framework of RANS family, RSM is known to predict turbulence behavior inside a cyclone with a better accuracy (Slack et al., 2003). Thus in the present study, Reynolds stress model (RSM) was chosen. It was observed that RSM required large number of iterations (about 7500 to 8000) for the solution to stabilize. This method of simulation implicitly has generated the low-pressure core around the cyclone axis without any additional definitions for air core.

For achieving the particle separation behavior inside the cyclone, Discrete Phase Modelling (DPM) technique was adopted. This method simulates the particle trajectory in a Lagrangian frame of reference. Stochastic tracking model was adopted for the dispersion of particles due to turbulence in the primary phase. The discrete phase formulation used in Fluent contains the assumption that the second phase is sufficiently dilute that particle–particle interactions and the effects of the particle volume fraction on the primary phase are negligible. In slurries with dilute concentrations of solids (particle concentration below 10% by weight) (Stovin and Saul, 1998), particle distribution behavior can be simulated using Lagrangian particle tracking approach. Thus in the present study particle tracking is carried out using the above methodology.

4. Experimental

The experimental setup consisted a slurry tank of 200 L capacity mounted on a stable platform. A centrifugal pump with 3-phase, 5.5 kw motor was connected to the slurry tank at the bottom. Feed slurry consisting of flyash material at different solids consistency was pumped into the cyclone body through the pipeline connected to the pump. The other end of the pipeline was connected to the inlet opening of hydrocyclone in study. The pressure drop inside the cyclone was maintained at required level with the help of by-pass arrangement actuated through a control valve on the pipeline. The pressure drop in the cyclone was measured with the help of a diaphragm type pressure gauge fitted near the feed inlet. The hydrocyclone was positioned upright above the slurry tank.

The experimental program was designed to achieve a wide range of water splits into the overflow and underflow products suitably selecting the spigot opening and feed inlet pressures. Hydrocyclone main body was fixed to the test-rig. Required opening spigot as per the experimental design was fitted to the hydrocyclone bottom. Initially, distribution studies were carried out by pumping water into the cyclone at different spigot openings and feed pressures. Required level of solids consistency was maintained in the slurry tank by mixing measured amount of flyash and water. Timed samples from overflow and underflow products were collected simultaneously in suitable containers. The underflow and overflow products collected were filtered, dried and weighed. Particle size distribution of representative samples of the dried products was analyzed using in Malvern laser particle size analyzer. Distribution points based on report of each size fraction in the feed to the underflow product were generated.

5. Results and discussion

5.1. Validation results

The experimental and simulation results of inlet flow rates (water entering the cyclone) and water-split (% report of total water into the overflow) into overflow product of 76 and 50 mm diameter hydrocyclone are presented in Table 3.

It can be observed from the table that the actual and simulated water throughput values obtained in a 50 mm hydrocyclone are found matching over a range between 0.42 and 0.45 kg/s. Similarly, the experimental values of water flow split into the overflow product varied between 75% and 97%. The simulated values of water split are found closely matching with the experimental results with error values below 3%.

The experimental flow rates through the feed inlet in the case of 76 mm hydrocyclone ranged between 1.16 and 1.32 kg/s. The simulated data is closely matching with the experimental values. The simulated throughput values are slightly lower numbers than the actual over the entire range. The actual and simulated values of water split in the 76 mm hydrocyclone indicate that a close matching is achieved over a range of water splits to overflow product between 33% and 95% with a marginal error of below 10%. Having understood close matching of the simulated results with the experimental values on water throughput

and splits, the simulated flow patterns in the cyclone in terms of static pressure and velocities are discussed.

5.2. Comparative flow behavior in 50 and 76 mm hydrocyclone

For clearer understanding on the effects of design geometries on the simulated flow patterns of 76 and 50 mm diameter cyclones, a comparative discussion is brought at comparable design conditions. Earlier experience on cyclones has indicated that among the design variables, spigot diameter influences the water throughput, split and flow characteristics most. Thus comparison is brought between the conditions where the ratio of the cyclone diameter and the underflow diameter is nearly matching. In the experimental designs studied the ratios of the cyclone diameter to spigot diameter were varied between 3.04 and 7.6 in case of 76 mm hydrocyclone and in case of 50 mm hydrocyclone, the ratios were varied between 5.32 and 15.6. For comparing the flow profiles inside the system, the conditions matching a design ratio of around 5.2, which corresponds to 15 mm spigot opening of 76 and 9.4 mm spigot opening of 50 mm hydrocyclones are selected. It is interesting to note that at these conditions, the water flow splits into the overflow are nearly matching (76.5% in 50 mm diameter and about 79.2% in 76 mm diameter hydrocyclones). The comparative discussions on the flow profiles of both designs are discussed as follows.

5.2.1. Static pressure
The static pressure inside the system basically decides the material flow in the radial and vertical direction within the cyclone. The simulated contours of static pressure in radial planes at different axial heights of 50 and 76 mm hydrocyclones are presented in Fig. 1. It can be observed from the figure that the pressure values are minimum near the central axis and maximum on the cyclone walls with progressive concentric layers of increasing pressures from core to the cyclone wall. It can also be observed from the figure that the pressure contours are more or less axisymmetric around the cyclone axis covering a large cyclone height. However, some kind of asymmetry is observed at vertical heights approaching the spigot opening.

Further to understand the difference in the static pressure values between these designs the maximum and minimum values obtained in a particular radial line are plotted against axial heights in Fig. 2.

Table 3
Experimental and simulated values of water throughput and split

Experiment and condition	50 mm diameter hydrocyclone								76 mm diameter hydrocyclone							
Spigot opening	3.2 mm		4.5 mm		6.4 mm		9.4 mm		10 mm		15 mm		20 mm		25 mm	
	Exp.	Sim.	Exp.	Sim.	Exp.	Sim.	Exp.	Sim.	Exp.	Sim.	Exp.	Sim.	Exp.	Sim.	Exp.	Sim.
Throughput (kg/s)	0.45	0.44	0.42	0.42	0.42	0.42	0.43	0.43	1.16	1.2	1.17	1.27	1.3	1.37	1.32	1.41
Water split (%)	96.3	97.7	94.5	92.8	89	90.5	76.5	79.1	94.8	85.3	79.2	86.9	55.9	61.3	33.0	40.5
Err. split (%)	1.38		1.68		1.44		2.6		9.51		7.66		5.36		7.51	

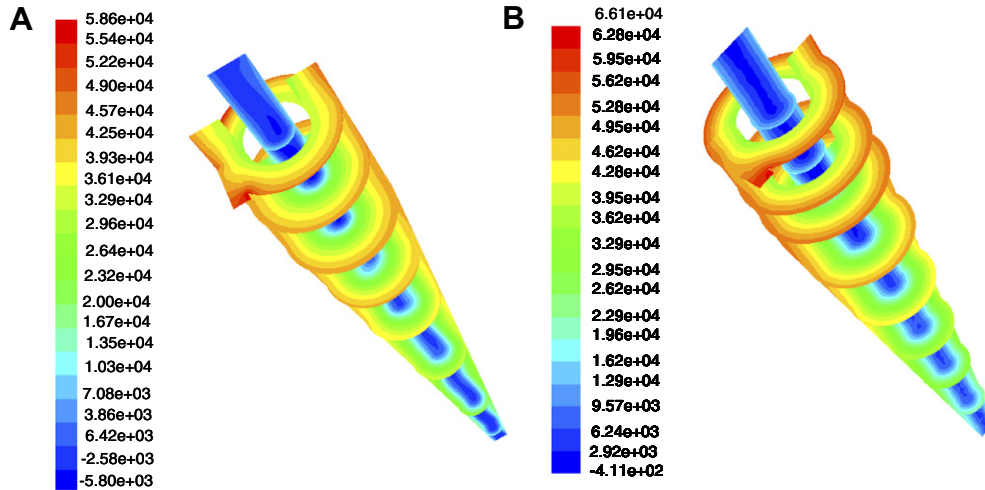Fig. 1. Static pressures at different axial heights and at central vertical plane: (A) 50 mm hydrocyclone design (D/D_u ∼ 5.3) and (B) 76 mm hydrocyclone design (D/D_u ∼ 5.1).
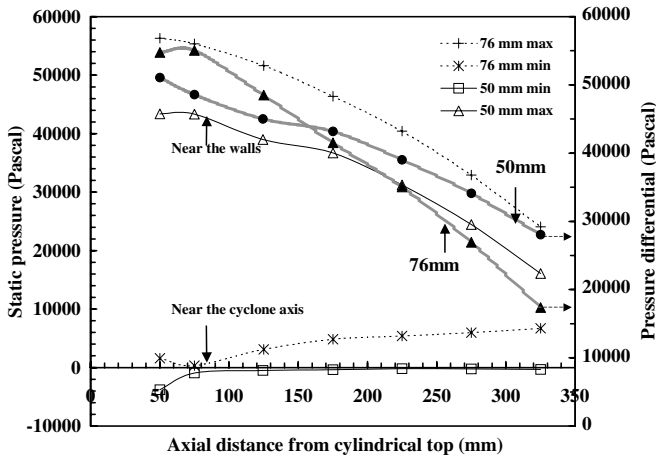

Fig. 2. Minimum and maximum values of static pressures at different axial heights.

From the figure the following observations can be made:

- Maximum values of static pressure (which are observed on the walls) decrease with increasing the cyclone height from the top to bottom in both the cases of 50 and 76 mm diameter hydrocyclone. This observation indicates the material flow in the downward direction along the cyclone walls.
- The minimum values of static pressure (which are observed around the cyclone axis) increase with increasing axial height from the top to bottom (50–325 mm from the base line) in both the cases of 50 and 76 mm diameter hydrocyclone. This indicates that relatively lower pressures are prevalent at axial heights near the vortex finder indicating material flow in the vertically upward direction at the core.
- The pressure differential between the minimum and maximum static pressure values (obtained at cyclone

wall and the axis, respectively) at different cyclone heights indicate that the pressure differential decreases from the top to bottom in both 50 and 76 mm diameter hydrocyclones indicating relatively lower radial inflows towards the cyclone axis.
- The pressure differential curves also indicate that the slope of the curve obtained for 76 mm diameter hydrocyclone design is high compared to a 50 mm diameter hydrocyclone design. Further it can be observed that till 150 mm axial height from the base line, the pressure differential values in 76 mm diameter hydrocyclone design are higher compared to a 50 mm diameter hydrocyclone. However, at heights beyond 150 mm from the base line, the pressure differential values are higher in case of 50 mm diameter hydrocyclone design. The observation indicates that in 76 mm diameter hydrocyclone body, classification of water to overflow predominantly takes place in the cylindrical and upper conical portion of the cyclone. In a 50 mm diameter hydrocyclone body radial movement of water takes place even at lower conical portion of the cyclone body.

Further, to analyze the static pressure values generated around the central core region, the values are captured at three different heights in the cyclone body. Assuming that the maximum air core diameter smaller than the vortex finder diameter, the static pressure values corresponding to positions between the zero radial point at the axis to the radial distance equivalent to vortex finder diameter are generated. Radial pressure distribution curves generated at three axial heights corresponding to the bottom most portion at the spigot opening, interface of the vortex finder and upper cylindrical portion and the top portion of the vortex finder of 50 mm cyclone is presented in Fig. 3.

It can be observed from the figures that the curves exhibit more or less axi-symmetric nature. The curves representing the vortex finder and the spigot opening (Fig. 3A
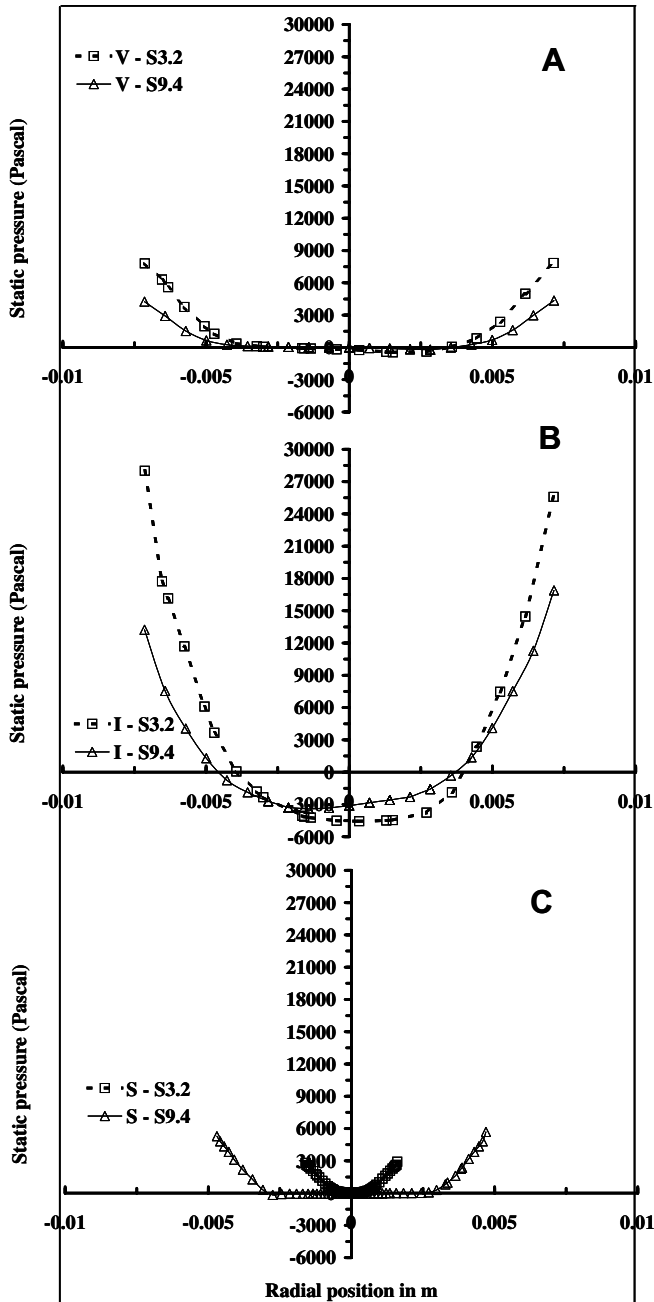
Fig. 3. Static pressure values at vortex finder outlet (A), interface of vortex finder and main cylindrical body (B) and at the spigot outlet (C) inside 50 mm hydrocyclone.

and C) are flat with static pressure equal to and below the atmospheric pressure, extending to some radial distance on either sides of the vertical axis. A steep increase in the curves can be observed on both the sides beyond the radial distance corresponding to zero static pressure, till the wall boundaries. It is expected that it is the flat zone indicating a zero static pressure and below is the air core. The exterior region within the vortex finder and the spigot openings is the zone through which water body is discharged. Due to the pressure differential between these individual layers in this region radial inflows are expected to occur both from the vortex finder outlet and also at the spigot opening.

It can be observed from the interface (Fig. 3B), that at the core, starting with a minimum low-pressure value near the cyclone axis, the static pressure reaches to zero value with increasing radial distance towards the wall. Beyond this radial point, the static pressure rapidly increases developing a maximum positive static pressure on the walls.

Unlike the vortex finder and the spigot outlets the interface is associated with a relatively low-pressure zone around the cyclone axis. This pressure differential between the outlet and the interface generates an axial inward flows both from the spigot and also from the vortex finder outlet. This observation is in agreement with the report by Narasimha et al. (2006) with their study using LES modeling approach.

It can be observed from the curves that the core diameter smallest at the spigot and maximum at the interface. At the vortex finder outlet it is more or less similar to the interface. The observation indicates that the air core entering through the spigot opening broadens till it reaches the region below the vortex finder and further maintains stability in the vortex finder. It can also be observed from the curves that at all the three positions the core diameter increases with increase in the spigot diameter indicating its device dependence. The increase in diameter is more at the spigot opening compared to interface and vortex finder. The core diameter observed at 15 mm spigot opening of 76 mm hydrocyclone is 9.2 mm, at 9.4 mm spigot opening of 50 mm diameter hydrocyclone it is about 5.4 mm and at 3.2 mm spigot opening of 50 mm diameter hydrocyclone it is about 0.6 mm.

5.2.2. Axial velocity

The axial velocity contours obtained in both 50 mm diameter and 76 mm diameter designs at different vertical heights and on central vertical plane are presented in Fig. 4A and B, respectively. It can be observed from the figures that an upward flow indicated by values of positive axial velocity can be observed around the cyclone axis. Negative axial velocity indicating downward movement along the cyclone wall could also be observed. Concentric layers of constant axial velocities can be observed along the radial planes at most part of the cyclone bodies. However at heights approaching the spigot opening, the contours exhibit some kind of non-axisymmetric nature. It can be observed from the figures that the positive values of axial velocity decreases till it reaches zero with increasing radial distance from the cyclone axis. With further increase in the radial distance, negative axial velocity begins and increases with increase in radial distance till the radial position near the walls. However, on the cyclone wall, the values of negative vertical velocity again decrease due to higher friction between layers of water body and cyclone wall. The observations can be better visualized from the Fig. 5A and B where the contours of positive and negative axial velocities obtained for 76 mm diameter hydrocyclone are separately presented. A thin boundary between these
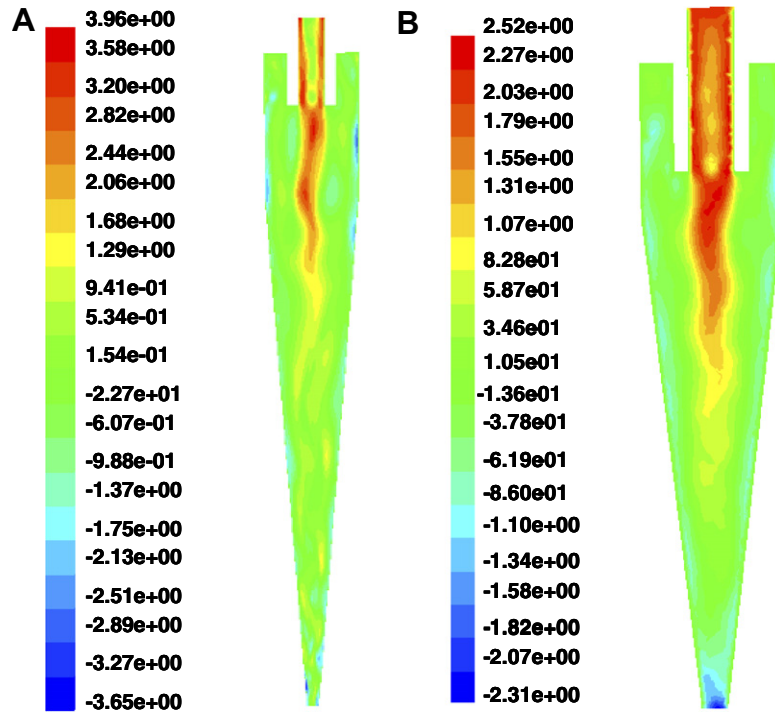
Fig. 4. Axial velocity contours at central vertical plane: (A) 50 mm hydrocyclone design (D/D$_u$ ∼ 5.3) and (B) 76 mm hydrocyclone design (D/D$_u$ ∼ 5.1).
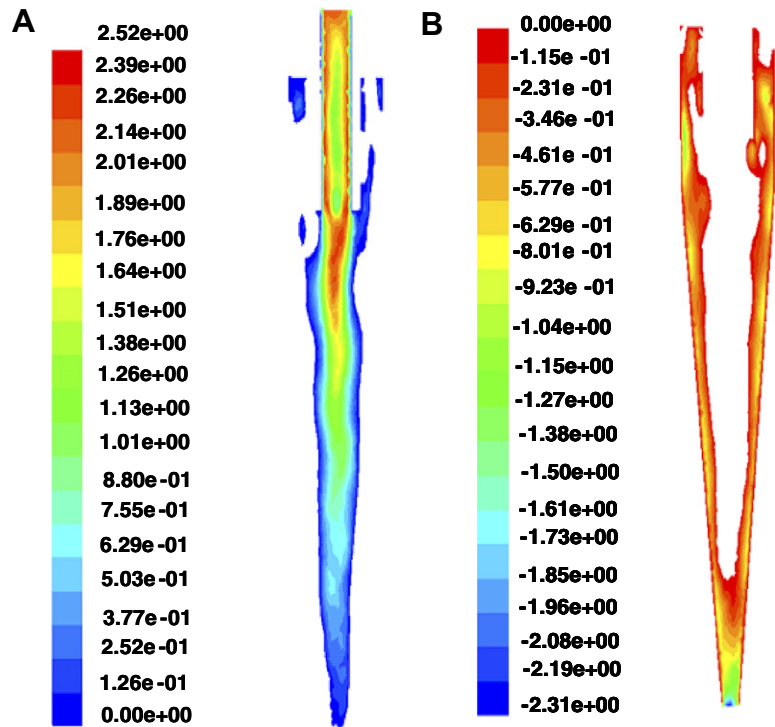

Fig. 5. Axial velocity contours in the vertical plane (76 mm diameter hydrocyclone design): (A) Positive (upward vertical flow) and (B) negative (downward vertical flow).

two layers is the zone of zero vertical velocity beyond which the regions of up and down ward flows exist.

Further, to examine the comparative results between these two geometries, the axial velocity data obtained along

the radial lines at different axial heights is presented in Fig. 6A and B. The figures indicate that the axial velocities in 50 mm diameter hydrocyclone design are higher in magnitude than the 76 mm diameter design hydrocyclone in
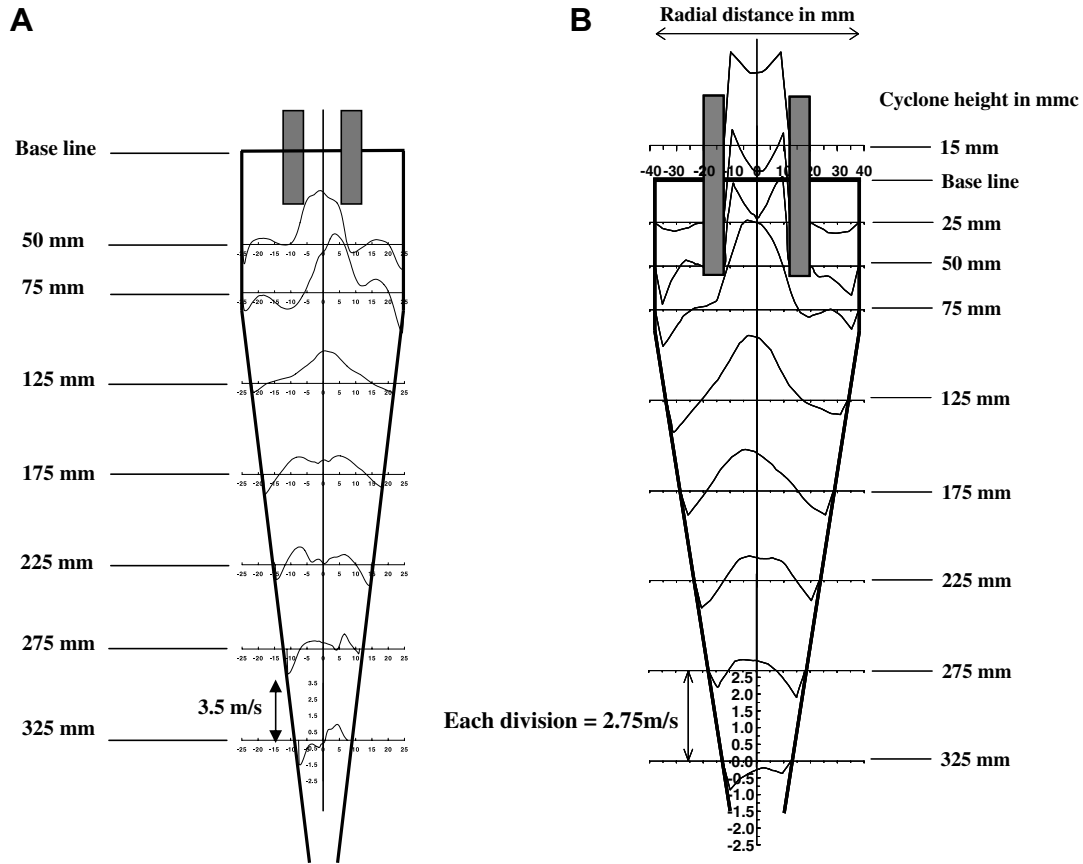
Fig. 6. Axial velocities along the radial lines at different axial heights: (A) 50 mm hydrocyclone design and (B) 76 mm hydrocyclone design.

both the positive and negative vertical directions. For instance, at an axial height of 125 mm, the maximum positive and negative velocities in a 50 mm hydrocyclone are 2.43 and −2.30 m/s and in 76 mm hydrocyclone design, the values are 2.01 m/s and −0.94 m/s. Similar observation can be made at different axial heights. It can also be observed that the difference in the negative axial velocities between the two designs is more predominant compared to positive velocities. This increase in the downward vertical velocity reduces the residence time for relatively coarser particles in the cyclone, a condition that reduces the cyclone cut size. Thus in a 76 mm hydrocyclone higher cut sizes are achieved in comparison with a 50 mm diameter hydrocyclone.

5.2.3. Tangential velocity

The tangential-velocity component of the continuous phase generates the centrifugal field force necessary for classification inside the hydrocyclone. The simulated results of tangential velocities in a 76 mm and a 50 mm diameter hydrocyclone at different vertical heights are plotted in Fig. 7A and B. The figures indicate that the tangential velocity increases with increasing radial distance from the axis till a maximum tangential velocity values is achieved. However at further increase in radial distances approaching towards the walls, the values decrease. The

observations made are similar to the reports of earlier workers in the literature (Slack and Wraith, 1997). The profiles of tangential velocity remain similar at different axial heights in the cyclone body in both the cyclones. In both the designs, the tangential velocities have maximum value in the cylindrical portion and minimum values are observed at lower portions in the cone near to the spigot opening. The observations indicate that at lower cyclone heights towards the spigot opening relatively lower centrifugal fields of force are generated and due to which in a hydrocyclone body the entrapped fine size fractions are re-oriented for progressive report into the vertical axial flow while treating solid materials (Cullivan et al., 2004).

5.3. Particle separation behavior

Distribution or partition curves (Wills, 1997) are generally used to describe the performance of hydrocyclone. Percentage report of different sized material in the feed to the underflow product is plotted against the size. The particle having a distribution value of 50% is referred to as d_{50} or cut size of the cyclone.

Particles are injected through the feed inlet into the cyclone body once the convergence of the primary phase is achieved. Sample group of 1000 particles of defined sizes
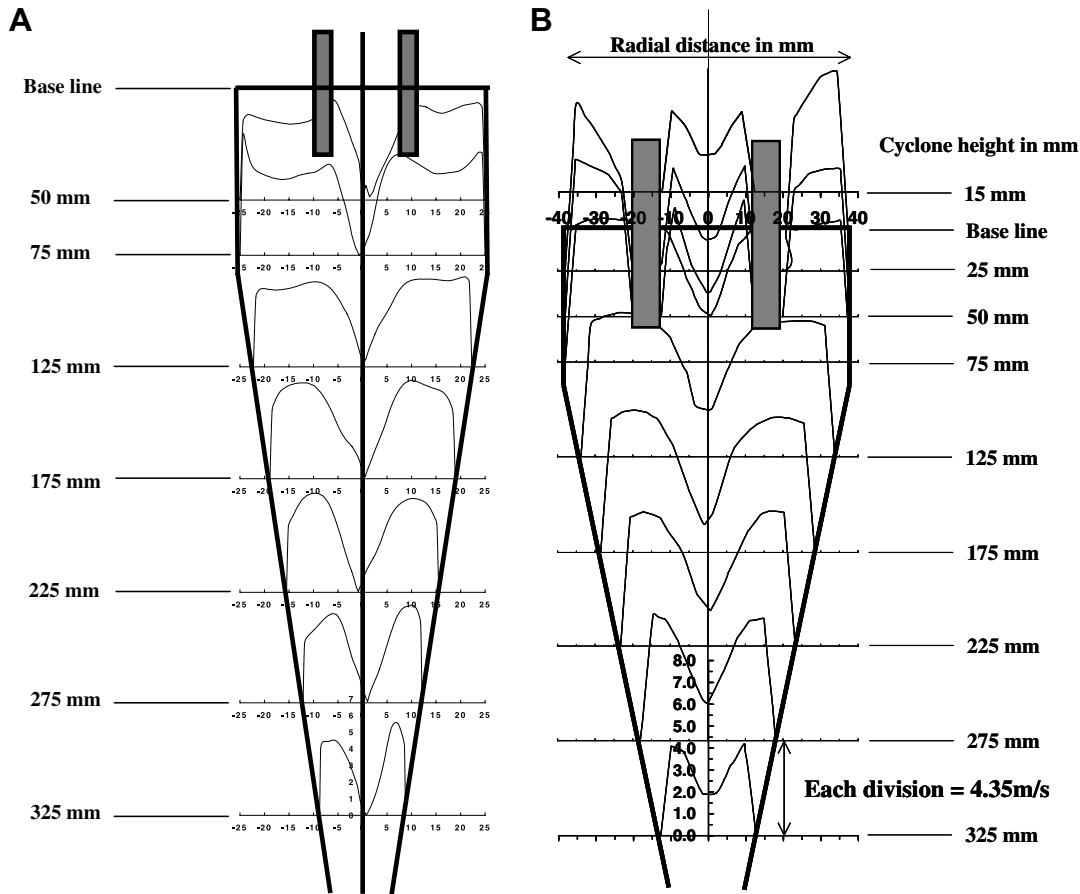
Fig. 7. Tangential velocities along the radial lines at different axial heights on central vertical plane: (A) 50 mm hydrocyclone design (D/D$_u$ ∼ 5.3) and (B) 76 mm hydrocyclone design (D/D$_u$ ∼ 5.1).

within a selected range were injected into the cyclone body through the feed inlet. The density of the material is maintained constant at 2300 kg/m^3 which corresponds to the density of flyash. Each time 10 sample runs were carried out and the report of particles into the overflow and underflow outlet streams were averaged. The partition numbers were obtained for each size in consideration.

5.3.1. 50 mm hydrocyclone

The partition curves obtained for different combinations of 3.2 and 9.4 mm spigot openings and by feeding slurries with 6%, 8% and 10% solids concentration are generated. These design conditions represent the narrowest and widest spigot openings used with 50 mm diameter hydrocyclone and thus they represent a range of flow splits. The partition curves generated for 9.4 and 3.2 mm spigot openings along with the simulated curve are presented in Figs. 8 and 9, respectively.

It can be observed from Fig. 8 that the experimental values of d$_{50}$ varied between 6.5 and 8.0 μm for feed concentration between 6% and 10% solids. An increase in the feed solids content has increased the underflow solids concentration between 19% and 31%. An increase in the solids concentration increases the viscosity of the fluid and a rise in the viscosity of the fluid reduces the air-core diameter

(Narasimha et al., 2006) diameter. A rise in the viscosity might have decreased the tangential velocity and in turn lowered the pressure drop at the spigot outlet. A reduced pressure drop might have reduced the air core diameter and increased the water report to overflow through displacement in the core region. Under the above condition, additional water might have carried relatively coarser fractions to join the vertically upward flow and hence increased the d$_{50}$ values.

It can also be observed from the figure that the simulated d$_{50}$ value at this design is 8 μm which is found matching with experimental conditions with error values varying between 22%, 12% and −1% for 6%, 8% and 10% solids/ respectively. It can also be observed from the figure that the d$_{75}$ values i.e., the size of the particle, which has 75% chances of reporting to the underflow product, is found varying between 10.2 and 11.9 μm. The simulated d$_{75}$ value at this design condition is 9.6 μm, which is smaller than the experimental values with error values varying between 6% and 24%. Higher error values are encountered at higher feed solids concentration. It can also be observed from the figure that the d$_{25}$ values i.e., the size of the particle, which has 25% chances of reporting to the underflow product, is found varying between 2.5 and 4.0 μm while the simulated value is 5.5 μm. It may be noted that though the
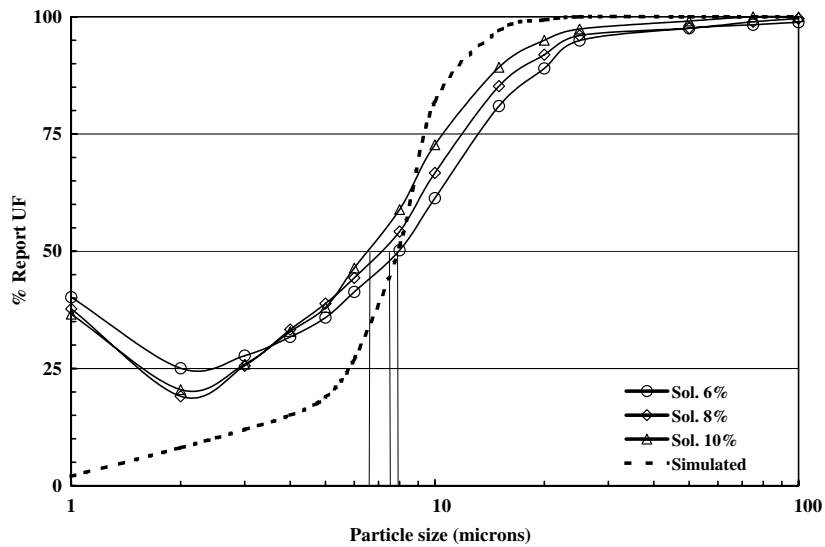
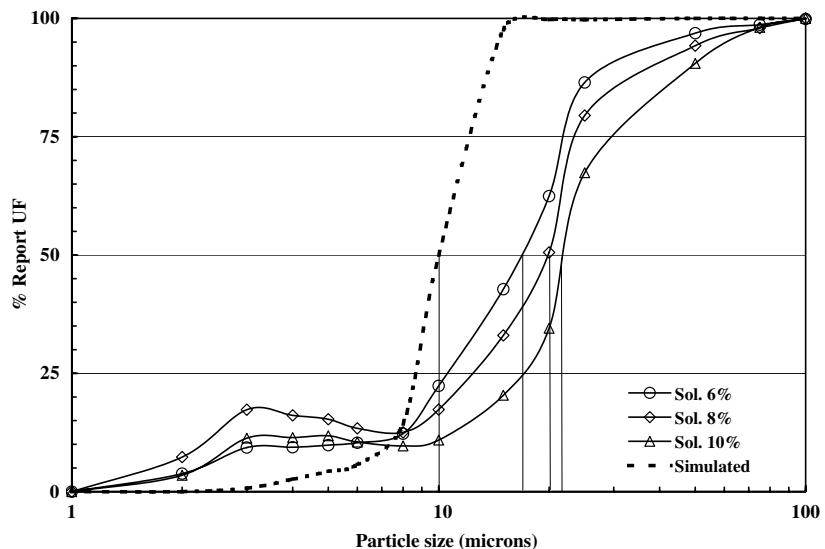Fig. 8. Partition curves obtained at 50 mm diameter hydrocyclone with spigot opening of 9.4 mm diameter.

Fig. 9. Partition curves obtained at 50 mm diameter hydrocyclone with spigot opening of 3.2 mm diameter.

error values between the actual and simulated results are found varying between 25% and 55%.

It can be observed from Fig. 9 that at the design condition corresponding to 3.2 mm spigot opening, there is a major divergence between the experimental and the simulated results. The simulated d_{50} value is about 10 μm. The experimental values of d_{50} are more than the predicted values. The values are found increasing between 12.5 and 21 μm for increase in feed solids concentration between 6% and 10%. The nearest d_{50} value matching at this design is 12.5 μm with an error value of about 25%, which is obtained at 6% solids concentration. The increased deviations can be explained due to increased solids concentration in the underflow product, which in the experimental product is found to vary between 53% and 56%. Increased viscosity at high solids concentration could have reduced

the core region and increased amounts of water splits through the overflow carrying relatively coarser fractions, and hence increased the d_{50} values.

5.3.2. 76 mm hydrocyclone

The distribution curves obtained at 76 mm diameter hydrocyclone with spigot openings of 10 and 15 mm diameter are presented in Figs. 10 and 11. The simulated d_{50} value at 10 mm spigot opening is 17.5 μm. The experimental d_{50} values at 6% and 10% solids this design condition (Fig. 10) are 17.7 and 19.4 μm, respectively. The experimental values deviate from the predicted value at 10% solids by 11% while at 6% solids the deviation is about 1% indicating a close match. The experimental values of d_{75} are found to be 24.5 and 26.2 μm at 6% and 10% feed solids concentration. The simulated d_{75} value is
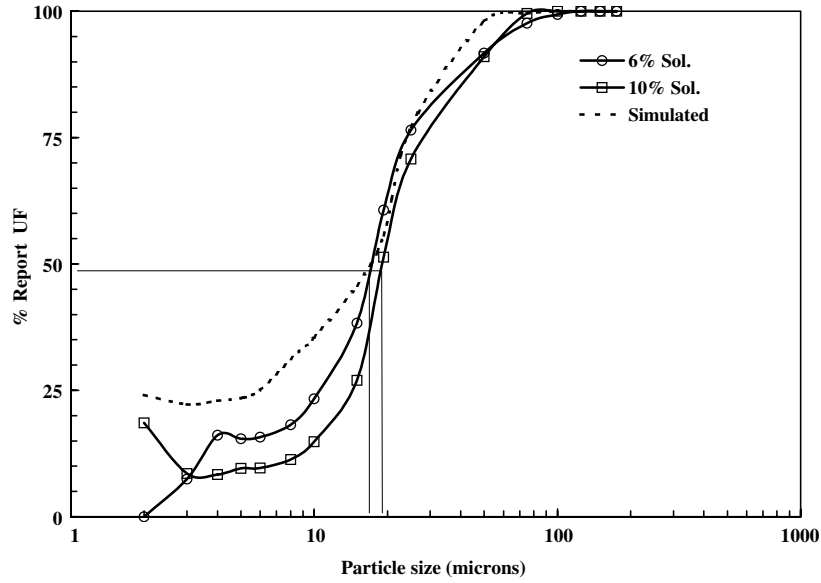
Fig. 10. Partition curves obtained at 76 mm diameter hydrocyclone with spigot opening of 10.0 mm diameter.
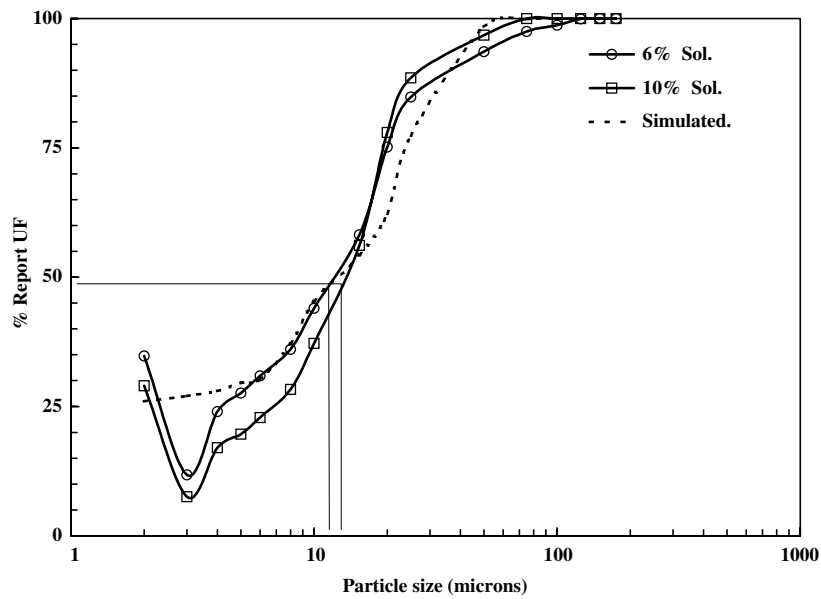

Fig. 11. Partition curves obtained at 76 mm diameter hydrocyclone with spigot opening of 15.0 mm diameter.

24.2% indicating a marginal deviation of 1.2% and 8.3% from the experimental values. However, the simulated d_{25} value is over predicted compared to the experimental values.

The experimental d_{50} values obtained at 15 mm spigot opening (Fig. 11) at 6% and 8% values are 13 and 15 μm, which are matching with the simulated d_{50} value of 13 μm with a maximum error about 4%. It can also be observed from the figures that the error values obtained at d_{75} size is well below 20% indicating a reasonably good prediction. It can further be observed from the figure that the error values obtained at d_{25} size considerably higher indicating over prediction of the distribution values. An

observation of the experimental results indicated that the solids concentration in the underflow slurry at 10 and 15 mm spigot openings and at 6% feed solids was around 55% and 21.7%. Similarly, at 10% feed solids concentration, the solids in the underflow product is 63% and 40%, respectively.

The matching characteristics of the experimental and simulated results can possibly be explained with the simulated values of the core diameter and available space for slurry discharge through the spigot. It is observed that in case of 50 mm diameter hydrocyclone, the core diameter is 5.4 and 0.6 mm at spigot openings corresponding to 9.4 and 3.2 mm in diameter, indicating a slurry discharge

opening of 2 and 1.3 mm around the periphery. Similarly, in case of 76 mm diameter hydrocyclone the core diameter observed at 15 mm spigot opening is 8 mm indicating the discharge opening of 3.5 mm around the periphery. In 76 mm diameter hydrocyclone due to wider opening for discharge of solids at the spigot, the effective influence of viscosity on the core will be diminutive when compared with 50 mm diameter hydrocyclone. However, the observation leaves some scope for research on the influence of increase in viscosity on available space for slurry discharge and on the core at different cyclone discharge conditions especially in particle-laden flows.

An observation of the Figs. 8–11 indicates that with decrease in spigot diameter, the cut size in general increases. As observed in the axial velocity profiles, at smaller spigot openings the velocities increase in both the axial directions. The magnitude of increase in the positive axial velocity is domineeringly higher than the decrease in the negative axial velocity and thus net higher water split is achieved. At higher water split, relatively coarser fractions are carried into the overflow, which increases the cyclone cut size.

Similarly, the tangential velocity values observed with 50 mm diameter cyclone are higher than the 76 mm diameter hydrocyclone. Higher tangential velocities increase the centrifugal forces. At higher centrifugal forces relatively finer particles also get chance to report towards the cyclone walls. Further these particles join the downward axial flow and hence decrease the average size in both the overflow and underflow products. Thus a reduced cut size is obtained in 50 mm diameter hydrocyclone.

6. Conclusions

- A CFD simulation and validation study on 50 and 76 mm hydrocyclone designs has indicated that the water distribution values in terms of throughput and split closely match with the experimental results at all cyclone design conditions.
- Diameter of the core portion associated with static pressure values below the atmospheric pressure is found to broaden from the spigot opening till the interface where the vortex finder joins the main cylindrical body and further the diameter remains more or less unchanged at the vortex finder outlet.
- The predicted axial velocities are higher at all the axial heights in a 50 mm hydrocyclone compared to 76 mm hydrocyclone.
- In case of 50 mm hydrocyclone, the simulated d_{50} values of flyash reasonably match with the experimental results when the spigot diameter is 9.4 mm. However, deviations are found at d_{75} and d_{25} values.
- At a spigot opening of 3.2 mm diameter, major deviation between simulated and experimental d_{50} values is observed.
- In case of 76 mm hydrocyclone, better predictions on d_{50} values are obtained at both the 10 and 15 mm spigot openings and at both 6% and 10% solids concentration in the feed slurry.
- Better predictions in case of 76 mm diameter hydrocyclone over 50 mm could be due to lesser influence of slurry viscosity on the air core due to increased free space for slurry discharge through the spigot opening.

References

Cullivan, J.C., Williams, R.A., Cross, C.R., 2003. Understanding the hydrocyclone separator through computational fluid dynamics. Transactions of the IchemE, Part A, Chemical Engineering, Research and Design 81 (A4), 455–466.

Cullivan, J.C., Williams, R.A., Dyakowski, T., Cross, C.R., 2004. New understanding of a hydrocyclone flow field and separation mechanism from computational fluid dynamics. Minerals Engineering 17, 651–660.

Delgadillo, A.J., Rajamani, R.K., 2005. A comparative study of three turbulence-closure models for the hydrocyclone problem. International Journal of Mineral Processing 77, 217–230.

Devulapalli, B., Rajamani, R.K., 1996. A comprehensive CFD model for particle-size classification in industrial cyclones. In: Hydrocyclones '96. Mechanical Engineering Publications, Ltd., London, UK, pp. 83–104.

Dyakowski, T., Williams, R.A., 1993. Measurement of particle velocity distribution in a vertical channel. Powder Technology 77 (2), 135–142.

Dyakowski, T., Hornung, G., Williams, R.A., 1994. Simulation of non-Newtonian flow in a hydrocyclone. Chemical Engineering Research and Design 72 (A4), 513–520.

Dyakowski, T., Nowakowski, A.F., Kraipech, W., Williams, R.A., 1999. A three dimensional simulation of hydrocyclone behaviour. Second International Conference on CFD in the Minerals and Process Industries. CSIRO, Melbourne, Australia, pp. 205–210.

Fluent Inc, 2002. Modeling Turbulence, Fluent 6.0 documentation, 10.43–10.52.

Grady, S.A., Wesson, G.D., Abdullah, M.M., Kalu, E.E., 2002. Prediction of flow field in 10-mm hydrocyclone using computational fluid dynamics. Fluid and Particle Separations Journal 14, 1–11.

Grady, S.A., Wesson, G.D., Abdullah, M.M., Kalu, E.E., 2003. Prediction of 10 mm hydrocyclone separation efficiency using computational fluid dynamics, Research article. Dept. of Chemical and Civil Engineering, FAMU-FSU College of Engineering, Tallahassee, and USA.

Griffths, W.D., Boysan, F., 1996. Computational fluid dynamics (CFD) and empirical modelling of the performance of a number of cyclone samples. Journal of Aerosol Science 27 (2), 281–304.

Hargreaves, J.H., Silvester, R.S., 1990. CFD analysis of deoiling hydrocyclone performance. Transactions Institute Chemical Engineering 68, 365–385.

Hsieh, K.T., Rajamani, K., 1988. Phenomenological model of the hydrocyclone: model development and verification for single-phase flow. International Journal of Mineral Processing 22 (1–4), 223–237.

Kelsall, D.F., 1952. A study of the motion of solid particles in a hydraulic cyclone. Transactions, Institute Chemical Engineers 30, 87–108.

Lynch, A.J., Rao, T.C., 1975. Modelling and scale up of hydrocyclone classifiers. 11th. International Mineral Processing Congress, Cagliari, pp. 245–269.

Malhotra, A., Branion, R.M.R., Hauptman, E.G., 1994. Modelling the flow in a hydrocyclone. The Canadian Journal of Chemical Engineering 72, 953–960.

Ma, L., Ingham, D.B., Wen, X., 2000. Numerical modelling of the fluid and particle penetration through small sampling cyclones. Journal of Aerosol Science 31 (9), 1097–1119.

Monredon, T.C., Hsieh, K.T., Rajamani, R.K., 1992. Fluid flow model of the hydrocyclone: an investigation of device dimensions. International Journal Mineral Processing 35 (1–2), 65–83.

Narasimha, M., Sripriya, R., Banerjee, P.K., 2005. CFD modeling of hydrocyclone—prediction of cut size. International Journal Mineral Processing 75 (1–2), 53–68.

Narasimha, M., Brennan, M., Holtham, P.N., 2006. Large eddy simulation of hydrocyclone; prediction of air core diameter and shape. International Journal of Mineral Processing 80 (1), August (2006), 1–14.

Nowakowski, A.F., Kraipech, W., Williams, R.A., Dyakowski, T., 2000. The hydrodynamics of a hydrocyclone based on a three-dimensional multi-continuum model. Chemical Engineering Journal 80 (1–3), 275–282.

Nowakowski, A.F., Dyakowski, T., 2003. Investigation of swirling flow structure in hydrocyclones. Transactions of the Institution of Chemical Engineers, Chemical Engineering Research and Design 81 (A), 862–873.

Nowakowski, A.F., Cullivan, J.C., Williams, R.A., Dyakowski, T., 2004. Application of CFD to modelling of the flow in hydrocyclones. Is this a realizable option or still a research challenge? Minerals Engineering 17, 661–669.

Pericleous, K.A., Rhodes, N., 1986. The hydrocyclone classifier—a numerical approach. International Journal of Mineral Processing 17 (1–2), 23–43.

Plitt, L.R., 1976. A mathematical model of hydrocyclone classifier. CIM Bull, 114.

Rajamani, R.K., and Milin, L., 1992. Fluid flow model of the hydrocyclone for concentrated slurry classification. Hydrocyclones: Analysis and Application: 4th Intentional Conference, vol. 12. pp. 95–108.

Schuetz, S., Mayor, G., Bierdel, M., Piesche, M., 2004. Investigations on the flow and separation behavior of hydrocyclones using computational fluid dynamics. International Journal of Mineral Processing 73 (2–4), 229–237.

Slack, M.D., Wraith, A.E., 1997. Modelling the Velocity Distribution in a Hydrocyclone, 4th International Colloquium on Process Simulation, pp. 65–83.

Slack, M.D., Boysan, F., 1998. Advances in cyclone modelling using unstructured grids. In: Scandinavian FLUENT UGM Gothenburg.

Slack, M.D., Prasad, R., Baker, A., Boysan, F., 2000. Advances in cyclone modelling using unstructured grids. Transactions Institute Chemical Engineers 78, 1098–1104.

Slack, M.D., Del Porte, S., Engelman, M.S., 2003. Designing automated computational fluid dynamics modeling tools for hydrocyclone design. Minerals Engineering 17, 705–711.

Stovin, V.R., Saul, A.J., 1998. A computational fluid dynamics (CFD) particle tracking approach to efficiency prediction. Water Science and Technology 37 (1), 285–293.

Suasnabar, D.J., Fletcher, C.A.J., 1999. A CFD model for dense medium cyclones. In: Second International Conference on CFD in the Minerals and Process Industries. CSIRO.

Udaya Bhaskar, K., Rama Murthy, Y., Ravi Raju, M., Sumit Tiwari, Srivastava, J.K., Ramakrishnan, N. In Press, doi:10.1016/j.mineng.2006.04.012.

Wills, B.A., 1997. Mineral Processing Technology, sixth ed., pp. 232–234.